International Journal of Hydrogen Energy 102 (2025) 1231–1242

Contents lists available at ScienceDirect

International Journal of Hydrogen Energy

journal homepage: www.elsevier.com/locate/he

Dynamic simulation of a highly load-flexible Haber–Bosch plant

Steffen Fahr [a,*], Robert Kender [b], Jan-Peter Bohn [b], Sebastian Rehfeldt [a], Andreas Peschel [c,d], Harald Klein [a]

[a] Technical University of Munich, TUM School of Engineering and Design, Department of Energy and Process Engineering, Institute of Plant and Process Technology, Boltzmannstr. 15, 85748, Garching, Germany
[b] Linde GmbH, Linde Engineering, Dr.-Carl-von-Linde-Straße 6-14, 82049, Pullach, Germany
[c] Forschungszentrum Jülich GmbH, Institut für nachhaltige Wasserstoffwirtschaft (INW-4), Am Brainergy Park 4, 52428, Jülich, Germany
[d] RWTH Aachen University, Aachener Verfahrenstechnik, Lehrstuhl für Prozess- und Anlagentechnik für chemische Wasserstoffspeicherung, Forckenbeckstr. 51, 52074, Aachen, Germany

ARTICLE INFO

Keywords:
Ammonia synthesis
Haber–Bosch process
Green ammonia
Power-to-X
Dynamic simulation
Flexible operation

ABSTRACT

The Power-to-Ammonia process has been suggested to decarbonize global ammonia production and to enable global energy trade using ammonia as a carbon-free energy carrier. Traditionally, Haber–Bosch plants for ammonia production based on natural gas have been operated near their nominal load and with slow load change rates. Power-to-Ammonia calls for more load-flexible plants to optimally utilize fluctuating renewable energy sources.

This work presents a detailed dynamic model of a modified Haber–Bosch plant including feed compression, reaction, separation, and refrigeration. We conduct simulation studies demonstrating load change rates up to 3%/min and safe operation with down to 10% of the nominal feed flow rate. Three strategies are investigated utilizing an increasing number of variables to achieve favorable conditions during part-load operation. Among those, a combination of pressure reduction, reduced flow in the synthesis loop, increased ammonia fraction in the reactor feed, and omitted intercooling between the reactor beds enables the smoothest load transition and best conditions during part-load operation. We further show that a moderate pressure reduction in the synthesis loop can reduce power demand during part-load operation.

1. Introduction

Ammonia is one of the most produced base chemicals globally. Today, ammonia is generally produced using fossil fuels (predominantly natural gas) as a source of hydrogen and energy and air as a source of nitrogen. It has been estimated that its production caused the emission of 450 megatons of carbon dioxide (CO_2) in 2019 [1]. The ammonia demand for existing use cases is expected to increase further within the next decades due to population growth and rising standards of living. Additionally, green ammonia is considered as a way to store green energy and transport it between continents [1,2]. Since ammonia does not contain any carbon, its use as a hydrogen carrier does not require any green carbon source or back-transport of CO_2 to achieve a closed carbon cycle. Moreover, its long-distance transport is established with 170 ships that can carry ammonia and are operational today [3]. Such ships can carry up to 50000 tons of ammonia [4] with a recent trend to even larger capacities.

Regardless of its use as a raw material or energy vector, ammonia production must be decarbonized in the near future to limit global CO_2 emissions. Using water electrolysis instead of fossil fuel-based processes as the hydrogen source eliminates virtually all direct carbon emissions from the process. However, it is paramount that the electricity used to power this *Power-to-Ammonia* process originates from carbon-free sources. For example, Salmon and Bañares-Alcántara [5] showed that even plants that source only around 10% of their power demand from the Australian power grid cannot satisfy the standards of the CertifHy low carbon certificate due to the indirect emissions associated with the power import. The certificate demands an approximately two-thirds emission reduction compared to the state of the art. The high indirect emissions, despite the low portion of power sourced from the grid, can be explained at least partly by the poor efficiency of burning coal or hydrocarbons for electricity production and then using that electricity elsewhere for water electrolysis.

Due to their vast power demand, Power-to-Ammonia plants are often considered along with their own dedicated green power supply. This allows optimal matching of the capacity of all components of the system. Various works have optimized Power-to-Ammonia plants

* Corresponding author.
E-mail addresses: steffen.fahr@tum.de, steffen.fahr@rwth-aachen.de (S. Fahr).

https://doi.org/10.1016/j.ijhydene.2025.01.039
Received 24 September 2024; Received in revised form 10 December 2024; Accepted 4 January 2025
Available online 15 January 2025

including wind and solar-based power generation, battery storage, hydrogen storage, an air separation unit (ASU), and a Haber–Bosch (HB) plant. Additional options include a grid connection that can cover the plant's power demand for short periods of low power production by wind and solar and fuel cells that produce power from stored hydrogen [5].

While intermediate storage options are available, they are often expensive and inefficient. Therefore, plants for which each component of the plant is highly load-flexible are usually advantageous with regard to the levelized cost of ammonia (LCOA). Electrolyzers are widely considered highly flexible both in their turn-down ratio and their load change rates. ASUs have recently been shown to be capable of performing fast load ramps (e.g., 50 to 100% main air compressor flow with a load change rate of 8%/min) [6]. The HB plant itself is generally considered the least flexible part of the process. To avoid large hydrogen buffer storage, future HB plants must become more load-flexible. Particularly the ability to run at low part load while avoiding a complete plant shutdown is attractive in this context. Mucci et al. [7] report cold starts of conventional plants to take up to several days, though mostly due to the steam reforming section. Nonetheless, cold starts of the HB plant itself require reducing the catalyst, which takes on the order of 24 h. Newly built green plants may potentially require only 12 h for a cold and as little as 10 min for a warm start [7].

Armijo and Philibert [8] demonstrated that depending on the energy mix and the location, the LCOA can be reduced by about 20% if the HB plant can ramp down to 20% and be shut down completely if necessary compared to a HB plant with a minimum load of 60% of its nominal load. Wang et al. [9] found a 30% LCOA reduction for a moderately flexible (60% minimum load) compared to a completely inflexible HB plant. A further reduction to 10% minimum load only improved the LCOA by up to 7.1%. Similarly, for off-grid plants, Campion et al. [10] achieved 20% lower LCOA with a minimum HB plant load of 40% compared to an inflexible plant but reported only negligible improvements with a further reduction in minimum load. However, it is notable that their hydrogen storage for 40% minimum load requires 10 ha of land, which may not be available for all brownfield plants.

Smith and Torrente-Murciano [11] chose a heuristics-based optimization approach for the scheduling and design problem instead of the linear programming approach used in the previously mentioned work. This enables the use of nonlinear equations, but takes away the guarantee of global optimality. In addition to conventional HB plants, they also considered potentially more flexible absorption-enhanced and single-vessel ammonia synthesis. Load flexibility of the ammonia plant was found especially beneficial for wind-dominated power profiles.

Salmon and Bañares-Alcántara [12] showed that a HB plant with a minimum load of 20% can reduce the LCOA by more than a third, compared to a completely inflexible HB plant. The majority (80%) of this reduction occurs when reducing the minimum load of the HB plant from 100% to 60%, with only a slight additional reduction for a more flexible HB plant. In addition to a linear programming-based design considering the power production profile over a year, the authors also conducted a simulation over a year with high-level model-predictive control (MPC) with a prediction horizon that was limited to 12, 24, or 48 h. They showed that the inevitably limited prediction horizon can lead to hundreds of plant shutdowns due to the battery or hydrogen storage running empty. These shutdowns are highly undesirable due to the long start-up time of HB plants and the fatigue caused by the procedure. Salmon and Bañares-Alcántara [12] were able to avoid these failures, e.g., by sizing the plant components assuming 40% minimum load and then operating the plant with down to 20% load. The important implication of this is the following: Being able to achieve very low part load during the actual plant operation can be extremely important to avoid unscheduled plant shutdowns. Meanwhile, assuming the same part load may only lead to small improvements in the objective of the design optimization, where production forecasts are perfect. This point is also illustrated by Florez et al. [13] showing the hydrogen storage state of charge over a selected time period. As a result of the integrated scheduling and design optimization, the storage is emptied completely, which means that with the slightest prediction error (e.g., an unexpected bad weather event), the HB plant would potentially be shut down.

While many aspects of the high-level scheduling and design problem have been considered in the previous literature, there appears to be less information available on the detailed plant behavior at the often-assumed low load. Various previous works at the process and unit operation level have considered steady-state models at one or more operating points [14–18]. Fahr et al. [14] and Cheema and Krewer [16] developed operating strategies that allow for plant operation at low part load considering the steady state only.

Rosbo et al. [19] investigated the dynamic operation of a quench-cooled ammonia synthesis reactor between 20 and 120% of its nominal hydrogen feed flow rate. The reactor was modeled as a one-dimensional plug flow reactor (PFR). Due to the heat recovery in the reactor system, it inherently possesses a feedback behavior that can lead to strong oscillations in the operating temperature. A PI controller for controlling the first bed inlet temperature was successfully used to suppress these oscillations.

Rosbo et al. [20] extended the analysis of Rosbo et al. [19] for other reactor types, i.e., adiabatic beds with indirect cooling in between and cooled tubular reactors. The operating variables of the steady-state reactor models were optimized for 30%–130% of the nominal load. Subsequently, the transient behavior of the reactor systems was discussed using dynamic simulations. Similar to the results of Khademi and Sabbaghi [17] for steady-state design models, the reactors with indirect cooling significantly outperformed the quench-cooled reactor, with the cooled reactor slightly outperforming the adiabatic beds with intercoolers.

Kelley et al. [21] considered a conventional HB plant with electric compressors for demand-side management. An efficient surrogate model was developed that uses linear dynamics and nonlinear algebraic functions that transform the input and output of the dynamic model. Using that setup, the authors were able to reduce the plant's operating cost between 1.39% and 3.70% by optimal scheduling in relative proximity to the nominal plant load.

Araújo and Skogestad [22] compared different control structures for a HB plant working at near-nominal conditions. They found operation at constant compressor speed to be advantageous, which corresponds to common industrial practice. As a result of this operating mode, the pressure fluctuates up and down with the plant load, while all other relevant process variables generally show a smooth and favorable trajectory during moderate load changes. Luyben [23] also suggested this mode of operation where the pressure "floats" up and down with the plant load. For green ammonia plants, which experience load fluctuations with both a higher frequency and a higher magnitude, this operating mode can no longer be maintained as it causes excessive fatigue in the equipment.

Kong et al. [24] successfully demonstrated a nonlinear model predictive control (NMPC) scheme for a HB plant operating between 50 and 100% load. The NMPC controller was able to maintain stable operation of the reactor while keeping the pressure within ±5 bar of the nominal pressure even with a step change from approximately 50 to 100% load. The loop pressure was controlled using the purge valve. However, the recycle compressor, which can significantly affect the pressure dynamics, was not modeled in detail with compressor maps.

It is known that high loop pressure can be maintained at a very low load by closing the purge and accumulating inert gas in the loop [25]. However, there is ideally very little inert gas present in green ammonia synthesis, which enables the use of a more efficient inert- and purge-free loop such as the one according to the Linde Ammonia Concept (LAC^{TM}) [26]. While pressure control via the purge is quite a direct and effective solution, it always comes with the drawback of the loss of reactants.

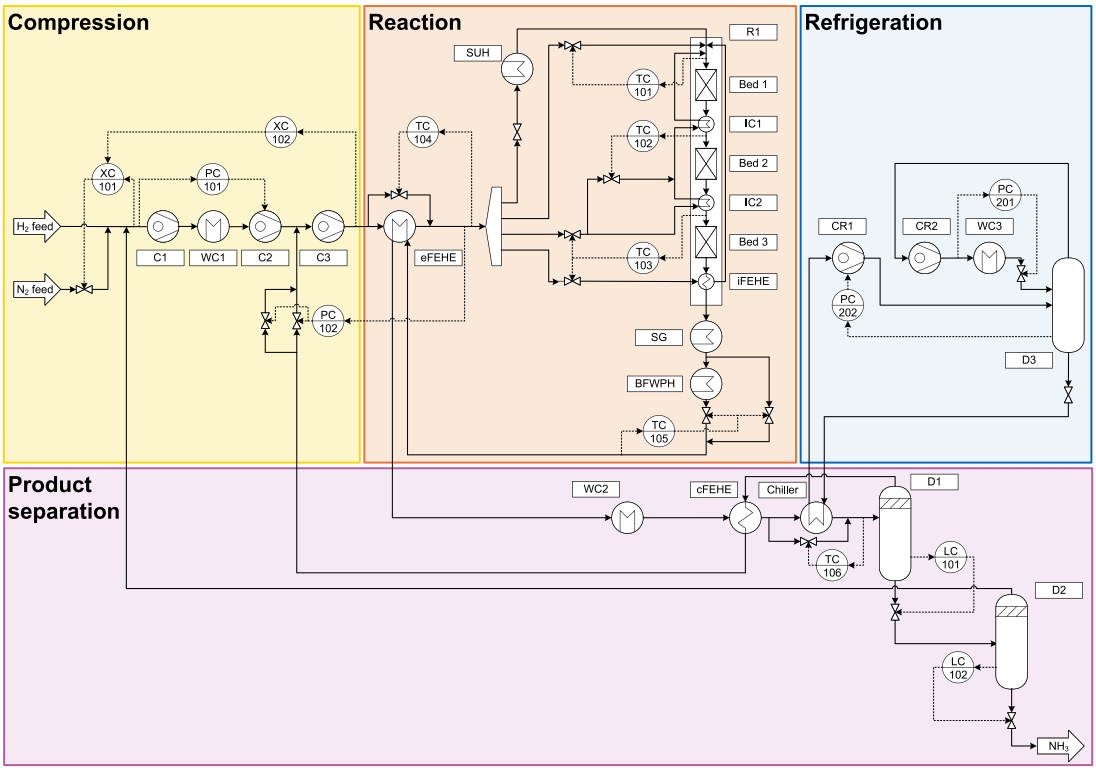

Fig. 1. Simplified process flow diagram (PFD) of the load-flexible HB plant.

This work investigates the dynamic operation of a purge-free ammonia loop between 10 and 100% load. While some works have considered the dynamic behavior during the design phase by using dynamic optimization with design degree of freedoms and suitable path constraints [27,28], our previous works [14,15] have only considered minimum and maximum load and have assumed that the transition is feasible. In this work, we use a reactor design obtained by the methodology of Fahr et al. [15] and show the feasibility of fast load changes between 10 and 100% load without major adverse events such as pressure and temperature spikes or reactor blow-out, which can lead to excessive fatigue and loss of production. To our knowledge, this load range has not been demonstrated on a detailed dynamic model before in the literature. We also include a refrigeration cycle for low-temperature product separation, which was not included in previous works that assumed high operating pressures at which ammonia can be condensed using cooling water [22–24].

The remainder of this work is structured as follows. First, we introduce the dynamic process model. Second, we discuss of the pressure dynamic of the synthesis loop, as this has not been discussed in detail in the literature before, and pressure control is a central aspect of our design and operation philosophy. Third, we demonstrate load changes between 10 and 100% load using three different operating strategies and discuss the load-dependent power demand of the HB plant. Finally, we discuss the simulation results in the context of typical assumptions on minimum load and load change rates taken in scheduling-focused works.

2. Methods

The HB plant is modeled in UniSim® Dynamics R491 [29] using the Peng–Robinson–Stryjek–Vera equation of state as the thermodynamic model. The ammonia synthesis process considered in this study can be divided into four sections, as depicted in Fig. 1.

First, in the compression section, the hydrogen and nitrogen feeds are combined with a small recycle from the medium-pressure (MP) flash D2 and compressed to a range of 100–150 bar. Each compressor stage includes an anti-surge controller and an associated recycle line. However, these are not shown in Fig. 1 for improved readability. The compressor stages are assumed to be driven by a single machine, i.e., their speeds cannot be controlled independently.

The reaction section is designed based on Fahr et al. [15] and consists of three adiabatic reactor beds with two intercoolers and an internal feed-effluent heat exchanger (iFEHE) designed for increased heat recovery during part load operation [15]. The reactor beds are modeled using the UniSim® PFR model and include heat loss terms from the beds into the annular gap between beds and shell and from the gap through the shell into the surroundings. We use the reaction kinetics from Fahr et al. [14], which have been developed to converge towards the correct reaction equilibrium when used in conjunction with the Peng–Robinson equation of state. By using reaction kinetics rather than an equilibrium model with a fixed equilibrium approach, we capture the effect of the retention time in the reactor beds on the approach to the equilibrium.

In the product separation section, the ammonia-rich synthesis gas is chilled and passes through two flash units at high and medium pressure, respectively. The vapor phase from the high-pressure (HP) flash is recycled to the last compressor stage, also referred to as the recycle compressor. The separation process is slightly simplified compared to industrial processes, where the product undergoes further purification in a low-pressure (LP) flash, and the product acts as the refrigerant for the chiller.

In contrast, the refrigeration process used in this study assumes a closed ammonia-based refrigeration cycle designed based on Flórez-Orrego and de Oliveira Junior [30]. We found that the energy consumption and part-load behavior of this process are comparable to the open refrigeration cycles typically used in ammonia synthesis. Unfortunately, there is a lack of literature on open refrigeration cycles, making it challenging to model accurately.

Fig. 1 also shows the basic control structure of the HB plant. We assume the hydrogen feed to be given by the upstream electrolysis

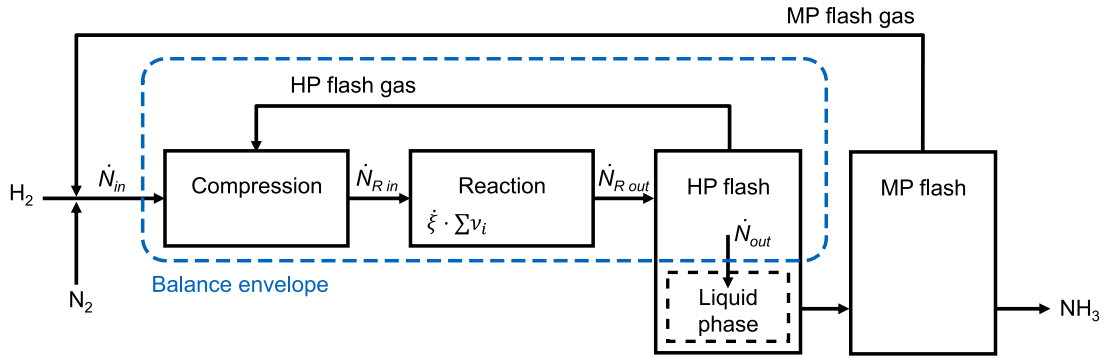

Fig. 2. Schematic representation of the balance envelope assumed for discussing the pressure dynamics in the synthesis loop.

plant and storage and, accordingly, define the plant load λ based on the hydrogen intake as

$$\lambda = \frac{\dot{M}_{\mathrm{H_2\ feed}}}{\dot{M}_{\mathrm{H_2\ feed,\ nominal}}} \,. \tag{1}$$

A definition based on the mass flow rate of ammonia out of the process would also be straightforward. However, the feed-based definition is better suited to represent the plant dynamics of green ammonia plants since it is directly linked to electrolysis and hydrogen storage in between. Note that these two definitions lead to identical numbers for the purge-free loop at steady state.

The compressor suction pressure is controlled via the compressor speed. The hydrogen-to-nitrogen-ratio in the synthesis loop is controlled using cascade control in order to react to disturbances in the feed flow quickly. The feed temperature of the reactor system is kept constant at 140 °C using a bypass over the external feed-effluent heat exchanger (eFEHE). As noted by Rosbo et al. [19], it would be ideal to control the reactor outlet temperature, which is more critical for catalyst degradation, but due to the slow response time, the reactor inlet temperatures are controlled instead. All controllers displayed in Fig. 1 are PI controllers.

For all non-integrating systems, step tests were performed, and the controllers were tuned using standard Ziegler–Nichols rules. Where necessary, the values of the tuning constants were further adjusted until desirable closed-loop step responses were achieved. For the temperature controllers TC101–TC105, we implemented controller gains and integral times as linear functions of the load to ensure stable operation at all loads. Accordingly, multiple step tests at different loads were performed.

Some of the controllers are designed as split-range controllers. For instance, the temperature controllers TC103 and TC105 send signals to two valves each. In both cases, one of the signals is inverted. For TC105, having only one valve in the bypass would lead to the valve being fully open while still not achieving the desired split between the bypass and heat exchanger at some operating points of the plant. Similarly, for TC103, two valves are necessary to cover all operating points and allow for part-load operation without any intercooling (see Section 3.3).

PC102 uses a small and a large valve to be able to pass the recycle flow with a low pressure drop at full load without operating at a low single-digit opening at part load. This is a common way to linearize valve behavior and prevent adverse behavior at low load. Here, we decided to start closing the small valve only below 50% controller output and fully closing the large valve at 33.3% and below with a linear relationship between the valve signal and the controller output.

As the pressure controller presents an important deviation from the state of the art, where the plant pressure is not controlled but adjusts itself according to the plant load [22,23], it is discussed in more detail here. To understand the underlying mechanism of our pressure controller, the mass balance around the gas contained in the synthesis loop needs to be considered.

As depicted in Fig. 2, we choose the system boundary carefully to include only the gas, as the mole amount N of gas present in a (constant volume) system is directly linked to the pressure p in the system by

$$p = \frac{Z\,N\,\bar{R}\,T}{V} \,, \tag{2}$$

with the compressibility factor Z, the universal gas constant $\bar{R}$, the (average) temperature T, and the system volume V. Accordingly, we draw the system boundary for this consideration such that the only entering stream is the stream entering the first compressor stage C1, $\dot{N}_{\mathrm{in}}$ in Fig. 2, and the only effluent stream is the mass flow leaving the gas phase by condensing in the chiller, $\dot{N}_{\mathrm{out}} = \dot{N}_{\mathrm{condensed}}$.

The balance of this system (in terms of moles of gas N_{gas} in the system) can be written as

$$\begin{aligned} \frac{dN_{\mathrm{gas}}}{dt} &= \dot{N}_{\mathrm{in}} - \dot{N}_{\mathrm{out}} + \dot{\xi} \sum_i \nu_i \\ &= \dot{N}_{\mathrm{in}} - \dot{N}_{\mathrm{out}} - \dot{\xi} \,. \end{aligned} \tag{3}$$

with the sum of the stoichiometric coefficients $\sum_i \nu_i = -1$ due to the volume-reducing reaction. In analogy to the typical definition of the reaction extent ξ, we define the reaction rate $\dot{\xi}$ as the rate of formation of ammonia, i.e., based on the reaction equation

$$0.5\ \mathrm{N_2} + 1.5\ \mathrm{H_2} \rightleftharpoons \mathrm{NH_3} \,. \tag{4}$$

Assuming approximately constant composition and average temperature within the system, we can further derive from Eqs. (2) and (3) that

$$\frac{dp}{dt} \propto \frac{dN_{\mathrm{gas}}}{dt} = \dot{N}_{\mathrm{in}} - \dot{N}_{\mathrm{out}} - \dot{\xi} \,. \tag{5}$$

It can be assumed that the ammonia formed in the reactor is condensed almost instantaneously due to the large flow rate compared to holdup, i.e., $\dot{N}_{\mathrm{NH_3\,out}} \approx \dot{\xi}$. The molar flow rate of gas leaving the system can be related to the component molar flow rate of ammonia leaving the system via the molar loading X_{diss} of dissolved gases in the liquid ammonia by

$$\dot{N}_{\mathrm{out}} = \dot{N}_{\mathrm{NH_3\,out}} \cdot \left(1 + X_{\mathrm{diss}}\right) \approx \dot{\xi} \cdot \left(1 + X_{\mathrm{diss}}\right) \,. \tag{6}$$

The molar loading X_{diss} is defined as the mole amount of dissolved gases (i.e., all components except for ammonia) divided by the mole amount of ammonia. Combining Eqs. (5) and (6) yields an approximate equation for the pressure change that, for an approximately constant (or sufficiently small) loading of dissolved gases, is only affected by the feed flow rate and the reaction rate:

$$\frac{dp}{dt} \propto \frac{dN_{\mathrm{gas}}}{dt} \approx \dot{N}_{\mathrm{in}} - \dot{\xi} \cdot \left(2 + X_{\mathrm{diss}}\right) \,. \tag{7}$$

For our further analysis, it can be helpful to expand the reaction rate $\dot{\xi}$ into the mass flow rate through the reactor and the change of ammonia mass fraction in the reactor. We use the mass flow here since the molar flow changes due to the reaction. The reaction rate $\dot{\xi}$ can be

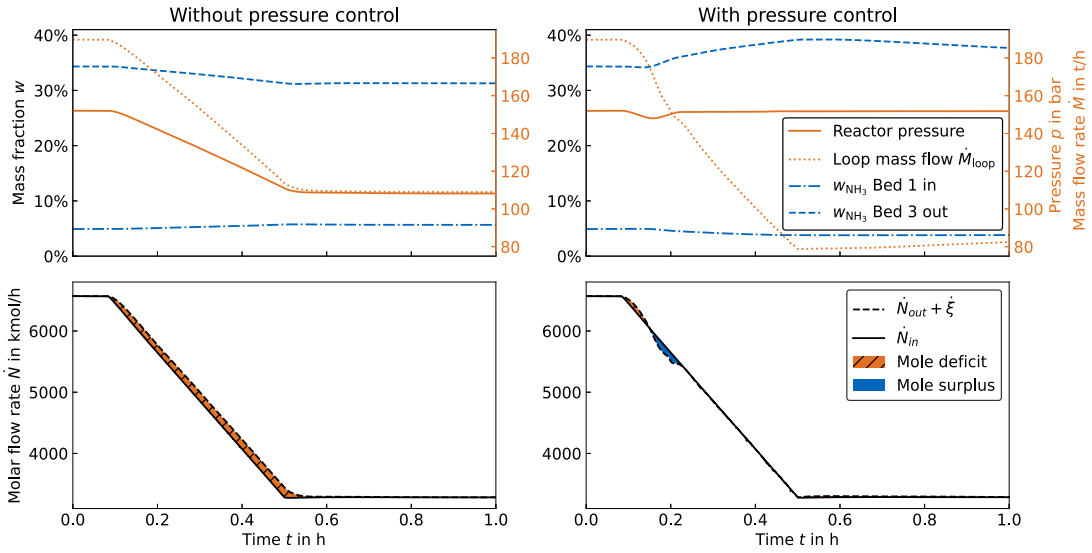

Fig. 3. Change in process conditions for a load reduction from 100 to 50% without (left) and with (right) pressure control. Pressure, loop mass flow and ammonia fraction before and after the reactor are shown in the top plots. The mass balance of the loop is visualized in the bottom.

related to the mass flow rate of ammonia formed $\dot{M}_{\mathrm{NH_3\,formed}}$ via the molar mass of ammonia $\bar{M}_{\mathrm{NH_3}}$, resulting in the expression

$$\dot{\xi} = \frac{\dot{M}_{\mathrm{NH_3\,formed}}}{\bar{M}_{\mathrm{NH_3}}} = \frac{\dot{M}_{\mathrm{loop}}}{\bar{M}_{\mathrm{NH_3}}} \cdot \left(w_{\mathrm{NH_3}\,R\,\mathrm{out}} - w_{\mathrm{NH_3}\,R\,\mathrm{in}} \right) , \tag{8}$$

where $\dot{M}_{\mathrm{loop}}$ is the mass flow rate through the reactor, and $w_{\mathrm{NH_3}\,R\,\mathrm{in}}$ and $w_{\mathrm{NH_3}\,R\,\mathrm{out}}$ are the ammonia mass fractions in the reactor feed and effluent, respectively. They correspond to the streams $\dot{N}_{\mathrm{NH_3}\,R\,\mathrm{in}}$ and $\dot{N}_{\mathrm{NH_3}\,R\,\mathrm{out}}$ depicted in Fig. 2.

This suggests that one way to avoid a pressure reduction in the system is to limit the flow through the reactor. The idea here is that the more gas flows through the reactor, the more ammonia is formed and condensed, and this directly affects the rate of pressure change according to Eq. (7).

Controlling the pressure via the recycle flow in the loop has also been suggested by Knudsen [31] and in a 2021 Haldor Topsøe patent [32] and will be adopted in this work. As will be discussed in more detail in Sections 3.3 and 3.4, the conversion in the reactor can also be limited (i.e., higher ammonia fraction in the reactor feed or lower ammonia fraction in the reactor outlet). However, this is only possible to a limited degree with conventional reactor design, as the released reaction heat required to sustain autothermal operation of the reactor is proportional to the conversion. By considering this low-load mode of operation during the design according to Fahr et al. [15], we can considerably lower the (per pass) conversion at part load. This does not affect the overall reactant conversion in the system, which is always close to 100% with the purge-free HB plant.

During operation, we employ elements of feedforward control by setting the setpoints for the pressure and optionally the bed 2 and 3 inlet temperatures and the chiller temperature according to the plant load. The setpoints are, in principle, interpolated between two loads based on the plant load λ with the aim of limiting the per-pass reactant conversion during part load.

During load changes, the plant load used for the interpolation is modified in order to delay or advance the setpoint ramps towards the load ramps. As the pressure controller's action is limited in one direction (increase the pressure by closing the valve), we ramp down the pressure setpoint with a slight delay (assuming 10% higher load for the interpolation) compared to the natural pressure reduction that occurs with a load reduction. This allows for a well-defined pressure trajectory rather than an uncontrolled pressure trajectory with fully open recycle valves. We also add a load-dependent bias directly to the pressure controller output in order to improve its performance. The underlying idea is that the valve is less open by default for a lower expected flow rate. This strategy resembles a simple version of the feedforward control described, e.g., by Liu et al. [33], and is common practice in the industry and especially useful in the absence of more advanced control strategies such as MPC.

In contrast to the pressure, we ramp the temperature setpoints with a positive bias; that is, during load changes, the setpoint ramps are advanced towards the load ramp. This proved favorable in reaching the desired conditions at the end of the load change despite the often slow dynamics of the temperature.

3. Results

In this section, we present our modeling results. First, we provide insight into the pressure dynamics of the HB plant and the suggested pressure control mechanisms. Then, we show load changes considering only the pressure setpoint to change with the load and otherwise constant setpoints. We further discuss two cases in which the per-pass conversion is lowered by operating the reactor without any intercooling with and without additionally increasing the condensation temperature in the HP flash D1. The three load change scenarios are inspired by previous works considering part load strategies in steady-state simulations [14–16] and are presented in the order from the simplest to the most complex in terms of the number of setpoint ramps involved.

3.1. Pressure dynamics

The mechanism behind the pressure reduction at part load and the suggested control mechanism are visualized in Fig. 3. The figure shows a selected set of variables during a load reduction from 100 to 50% load without (left) and with (right) pressure control in place. The load reduction begins at 5 min and ends at 30 min, as can be seen from the feed flow rates in the bottom figures.

The left portion of the figure shows the mechanism behind the pressure reduction during a load reduction. The lower portion shows that there is a discrepancy between the feed flow $\dot{N}_{in}$ and the two sink terms from Eq. (5). This temporary deficit in gas leads to a pressure reduction in the loop. As a result of the pressure reduction and the reduction in feed flow, the compressor speed is reduced by PC101. Moreover, the density of the gas in the loop is reduced. Both of these effects reduce the mass flow conveyed by the recycle compressor. The

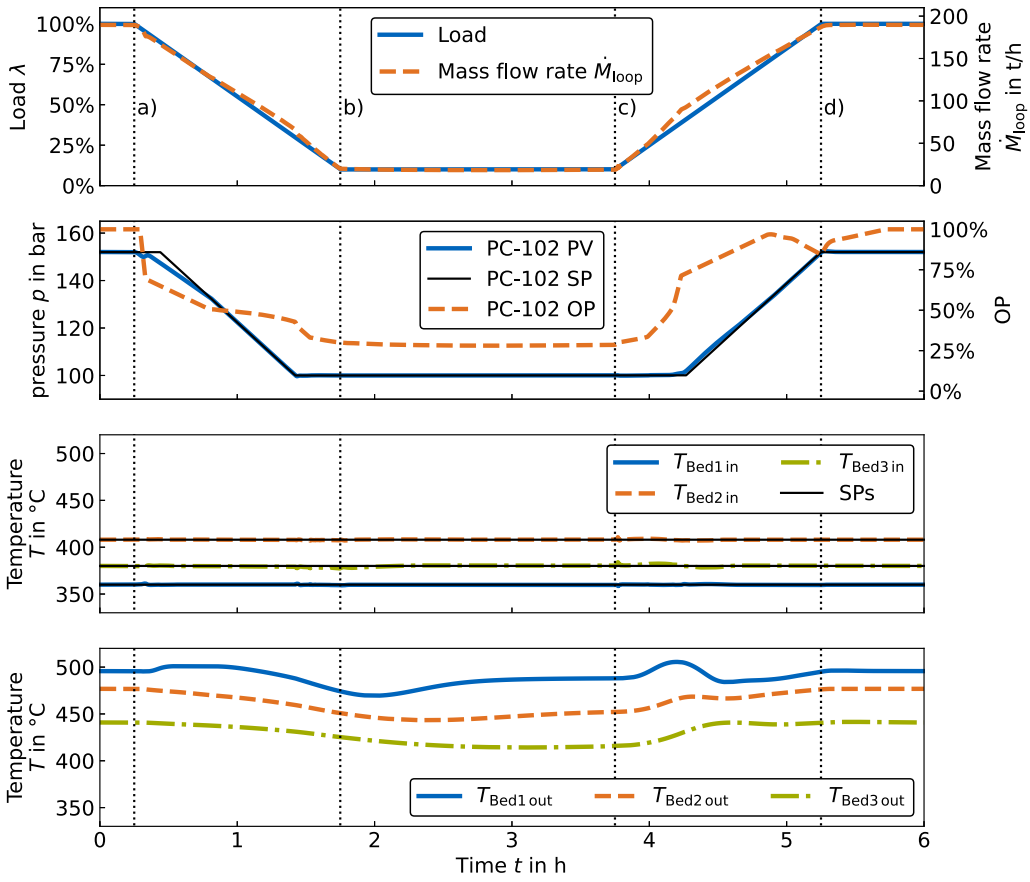

Fig. 4. Variable trajectories of a ramp-down followed by a ramp-up, each conducted with a load change rate of ±1%/min. All setpoints except for the pressure setpoint are held constant.

conversion in the reaction is also affected by the lower pressure. As a result of these effects, the reaction rate in the reactor decreases, and a new steady state is reached, in which the mass flow of gas eliminated by the reaction and condensed is again equal to the feed.

As can be seen in the right portion of Fig. 3, the flow through the reactor is reduced more compared to the case without pressure control. This is a result of the pressure controller acting on the recycle valve. Thereby, the rate of formation of ammonia, $\dot{M}_{NH_3\,formed}$, can be lowered, holding the balance between the feed flow rate and the condensation rate. Note that the higher conversion in the reactor due to the longer residence time (as seen by the ammonia fractions in the top right panel of Fig. 3) does not fully compensate for the flow reduction.

The pressure control method can be summarized as follows: If the feed flow rate $\dot{N}_{in}$ of the HB plant is given according to the load, then the balance equation Eq. (7) can only be affected by the reaction rate $\dot{\xi}$, which is readily modified with very little time delay by changing the valve position of the valves in the recycle and thereby affecting the parameters in Eq. (8).

3.2. Load changes with constant temperature setpoints

The trajectories in the following are given for standardized load changes down from 100% to 10% load, a holding period, and back up to 100%. The start and end of each load change are denoted by the letters a)–d) according to Table 1.

Fig. 4 shows selected variable trajectories for a load change rate of 1%/min. At the top, the load as defined in Eq. (1) is shown along with the mass flow rate into the reactor. Below, the process variable (PV), setpoint (SP) and output (OP) of the loop pressure controller PC102 are given. The bottom two plots show the bed inlet and outlet temperatures, respectively. As the inlet temperatures are controlled by TC101 - 103, we also provide the setpoints for reference.

It is apparent that the loop mass flow rate is reduced almost proportionally to the load, i.e., at 10% load, the loop also experiences only 10% of the mass flow. This means that the conversion in the reactor remains virtually constant, as the longer residence time and the lower pressure cancel out in terms of their effect on conversion. While a decrease in pressure reduces the per-pass conversion by shifting reaction equilibrium towards the reactant side, a reduced mass flow rate increases the conversion by reducing the approach to the equilibrium. At 10% load and 100 bar, these two effects almost cancel each other out with the operating strategy used here.

As explained in Fahr et al. [14], we assume that the pressure can be reduced to 100 bar during part-load operation. Not only does this reduce the electric power consumption at part load (as discussed in Section 3.5), but it also mitigates the risk of damaging the catalyst due to increased catalyst temperatures as the reaction conversion — and with it the temperature increase — in adiabatic beds is limited by the chemical equilibrium. For instance, below a pressure of about 125 bar, a violation of an upper catalyst temperature limit of 500 °C can be completely suppressed by entering the catalyst bed at no more than 350 °C [14]. In practice, the upper temperature limit is specific to the employed catalyst and usually proprietary information provided by the catalyst manufacturer. Values reported in the academic literature range from 500 to 530 °C [16,34]. We chose a temperature of 520 °C as our axes limits in the all figures below, which was not exceeded in any of the simulations.

As shown in the second plot of Fig. 4, the pressure trajectory perfectly follows its setpoint. Since the bed inlet temperature setpoints are kept constant, the bed outlet temperatures (bottom) fluctuate slightly during the load changes, eventually returning to values around 5–15 K below their full-load value at part load. The slight decline in the exothermic reaction is due to the pressure reduction as described above.

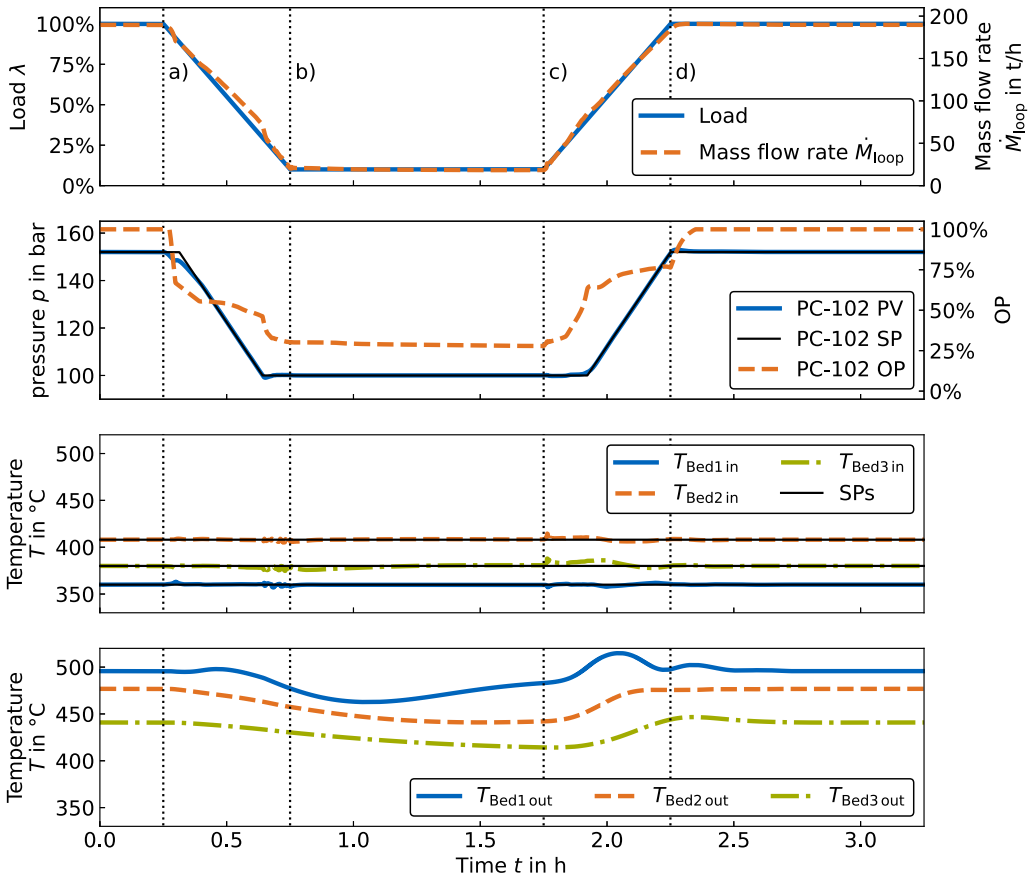

Fig. 5. Variable trajectories of a ramp-down followed by a ramp-up, each conducted with a load change rate of ±3%/min. All setpoints except for the pressure setpoint are held constant.

Table 1
Overview of characteristic moments in variable trajectories.

a)	Start of ramp-down
b)	Stop of ramp at 10% load
c)	Start of ramp-up
d)	Stop of ramp at 100% load

The above load change rate of 1%/min is the same as the one used by Rosbo et al. [19] for a load change between 20 and 100%. It generally compares favorably with the assumptions made in the previous literature. Allman et al. [35] assumed only 4% of ramp-up and 10% of ramp-down to be possible every 4 h in their scheduling program. Armijo and Philibert [8] limited the load change rate to ±20%/h (0.333%/min) based on interviews with manufacturers. Verleysen et al. [36], Florez et al. [13], Wang et al. [9], and Smith and Torrente-Murciano [11] also adopted this value. Salmon and Bañares-Alcántara [5] assumed load change rates of 20%/h for ramp-down and 2%/h for ramp-up. Salmon and Bañares-Alcántara [12] assumed load change rates of 20%/h for ramping down and 5%/h for ramping up but also considered up to the tenfold rate, which is up to 3.33% min of ramp-down rate, in a sensitivity analysis.

In the recent years, an increasing number of sources cite more ambitious goals for the load change rates of HB plants. For instance, Casale claim load change rates upward of 100%/h [37] and Topsoe claim to achieve 3%/min [38]. Beach et al. [39] demonstrated rapid load changes on a bench-scale adsorption-enhanced ammonia loop achieving a load increase of 25% in approximately one minute. Being capable of performing such rapid load changes is not strictly necessary if enough battery or hydrogen buffer capacity are available. However, they allow to exchange electricity or hydrogen storage for much cheaper ammonia storage. For instance, when running at full load in the day and minimum load at night with a load change rate of only 1%/min, the plant would be in the middle of a load change for an eighth of each 24 hour day, which is likely far from optimal operation.

Thus, even a load change rate of 1%/min can be considered rather slow when the load profile is dictated by daily fluctuations in the availability of renewable power. We therefore demonstrate the feasibility of more rapid ramps at 3%/min in the following, which is the same rate that Topsoe claim to be capable of [38]. The feasibility of the fast load changes shown in the following implies that of slower ones, which are generally easier to achieve.

Fig. 5 shows the dynamic variable trajectories for load changes according to the same strategy as used in Fig. 4 but at a load change rate of 3%/min. The pressure controller still tracks its setpoint well, as do the bed inlet temperature controllers. However, a closer look reveals a slight oscillation of about 1 K around the end of the ramp-down. This can be traced back to the tenfold reduction in mass flow rate in the loop (top plot), which significantly changes the system behavior and leads to oscillations despite the gain scheduling we implemented.

Naturally, the bed temperatures change faster with the faster load change rate compared to 1%/min, which can have implications for their durability. The outlet temperatures (bottom plot) also fluctuate slightly more during the fast ramp-up compared to the slower one.

3.3. Load changes without intercooling

The reduction in reactor mass flow rate not only poses a challenge to conventional control and brings the instruments (valves) involved close to their limits (fully opened/fully closed), but it can also lead to poor gas flow distribution in the reactor. This is not captured by our 1-dimensional model but is relevant for plant operation. According

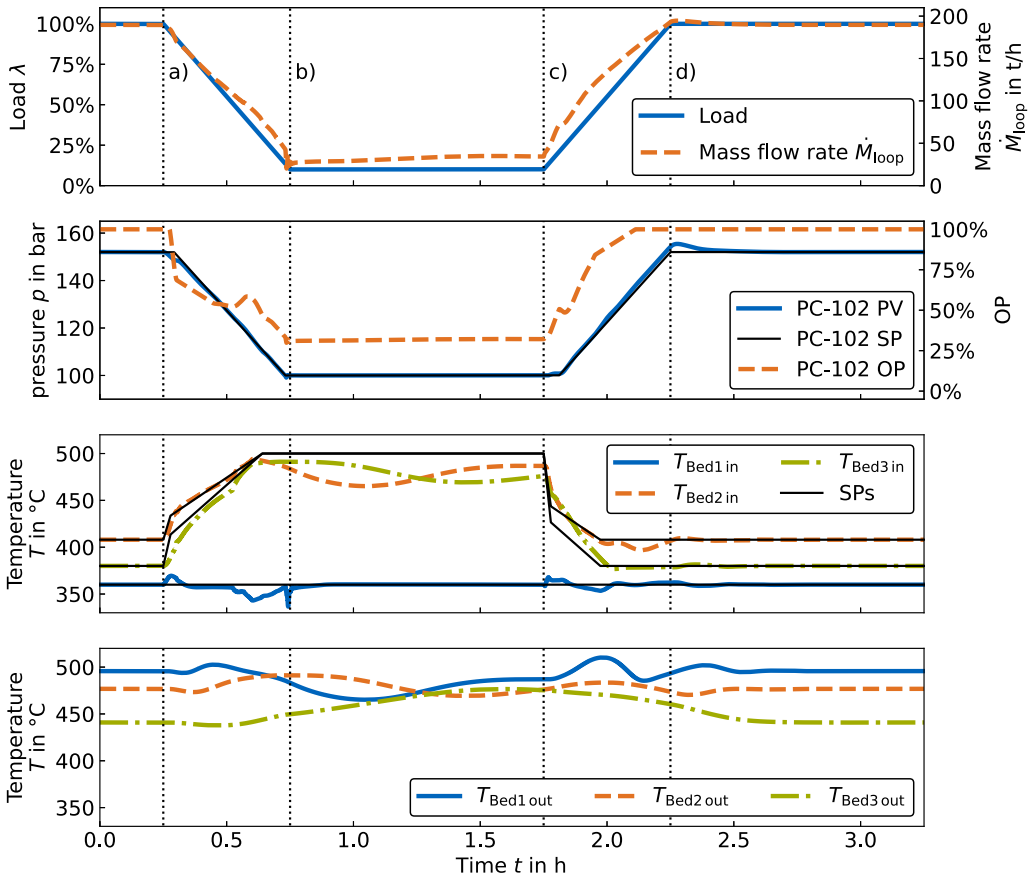

Fig. 6. Variable trajectories of a ramp-down followed by a ramp-up, each conducted with a load change rate of ±3%/min. The Bed 2 and Bed 3 inlet temperature setpoints are ramped such that intercooling is stopped at part load.

to Eq. (8), the same reaction rate $\dot{\xi}$, and thereby the same load, can be reached at higher loop flows $\dot{M}_{loop}$ by reducing the ammonia mass fraction $w_{NH_3\,R\,out}$ in the reactor effluent. One way to achieve this is to stop the cold gas flow through the intercoolers, thereby turning three adiabatic beds into one [14]. This mode of operation can also be though of as a "hot standby" of the second and third bed, where they are kept at temperature without producing significant amounts of ammonia. This is advantageous compared to bypassing these beds, as bypassing them would lead to them cooling down, which would impede fast ramp-up from low loads.

To ensure a smooth transition, the Bed 2 and Bed 3 inlet temperatures were ramped up to a point where the intercooling stops completely (see Fig. 6). The entire load change, again, takes place without any major fluctuations in the bed outlet temperatures and the pressure. It can also be seen in the top portion of the figure that a significantly higher reactor flow can be maintained compared to Fig. 5. However, due to the slow dynamics of the bed temperatures, the loop flow initially declines nearly as far as it does in Fig. 5 at time (b) and takes about 0.7 h to come back up to approximately double the flow compared to Fig. 5.

It must also be noted that due to the time it takes for the bed temperatures to stabilize at their full-load condition, the pressure slightly overshoots its full-load pressure after the ramp-up. This effect is much more pronounced if the temperature setpoints are ramped down linearly without the bias described in Section 2. While we deem the small pressure peak unproblematic in the context of the dynamic operation of the HB plant, it shows a potential limitation on load change rates for the ramp-up. Interestingly, Salmon and Bañares-Alcántara [5] and Salmon and Bañares-Alcántara [12] assumed a lower load change rate for ramp-up than for ramp-down, which confirms that the ramp-up is more limited.

Another drawback of this strategy is that around the end of the ramp-down, TC-101 controlling the inlet temperature of the first catalyst bed is saturated and the temperature temporarily falls below its setpoint down to 343 °C. Often, a lower temperature limit of 350 °C is considered to avoid reactor blow-out [14]. This limit represents a conservative assumption and is briefly violated here without causing reactor blow-out. At the significantly higher retention time of the reactor, it tolerates lower temperatures and associated slower kinetics without extinguishing. Moreover, the violation could likely be avoided by optimizing the temperature setpoint ramps, as it does not occur with any other strategies, despite the generally lower reaction heat released with the strategy described in Section 3.4. The second dip in the temperature profile is very brief and is a result of the conventional control structure used. This brief decrease in inlet temperature is tolerated due to the high thermal inertia of the reactor.

3.4. Load changes without intercooling and with increased NH_3 recycling

The fluctuations in Bed 2 and Bed 3 inlet temperature possibly promoting equipment fatigue and the temporarily still quite small reactor mass flow rate can be considered drawbacks of the part load strategy discussed in Section 3.3. These drawbacks can be at least partially overcome by combining the strategy with an increased condenser temperature, facilitating a high ammonia inlet fraction $w_{NH_3\,R\,in}$. Not only does this allow for a higher loop mass flow rate according to Eq. (8), but it also shifts the reaction equilibrium to a lower temperature, lowering the inlet temperatures of Bed 2 and Bed 3 at part load and thereby their temperature fluctuations, as shown in Fig. 7. On the other hand, the outlet temperature of Bed 1 is now significantly lower during part-load operation due to the inhibition of the reaction by the ammonia that is already present in the reactor feed.

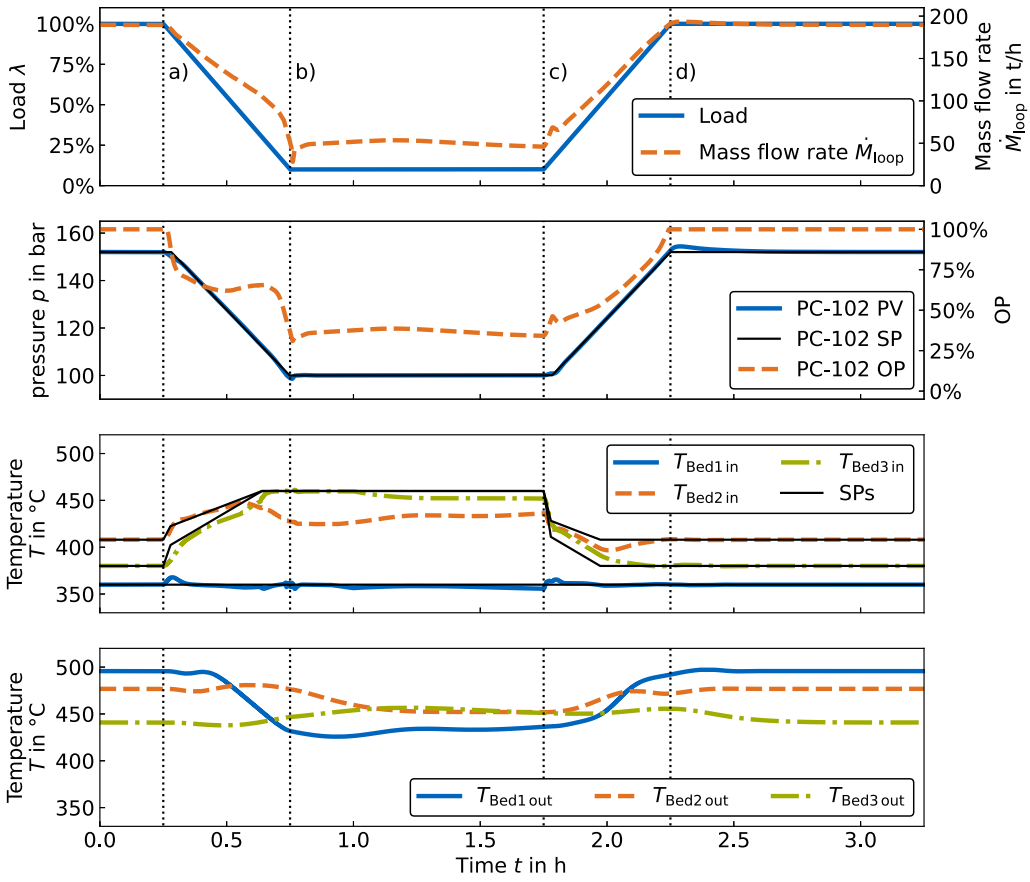

Fig. 7. Variable trajectories of a ramp-down followed by a ramp-up, each conducted with a load change rate of ±3%/min. The Bed 2 and Bed 3 inlet temperature setpoints are ramped such that intercooling is stopped at part load and the ammonia inlet fraction of the reactor feed is increased by increasing the condenser temperature.

The pressure trajectory, again, lacks any undesirable fluctuations and, due to the reduced change in bed temperatures, shows less of a pressure peak after the ramp-up.

3.5. Power consumption

We previously argued that the pressure reduction, in addition to avoiding a temperature violation in the reactor beds, allow for a reduction in the power consumption of the HB plant [14]. This effect is visualized in Fig. 8. The figure compares the total power consumption of the HB plant (excluding electrolysis and ASU) at part load if the pressure controller is set to 100 bar, 127.5 bar, and 152 bar. For all cases, we used the part load strategy described in Section 3.4. For comparison, the right bar shows the power consumption at full load.

As can be seen in Fig. 8, the power consumption is barely reduced at part load if the loop pressure is maintained. This is because the compressor has only a limited capacity to reduce its speed at the given pressure difference without entering the surge region. Therefore, the anti-surge controllers step in and limit the reduction in flow through the individual compressor stages, keeping the conditions overall similar to those at full load.

Since surge lines typically move to lower flows with lower pressure ratios, the anti-surge controllers allow for a lower flow at part load if the loop pressure is reduced. The combination of a lower pressure ratio and a lower flow allows for the compressor power to be reduced almost by half at part load. In other words, the operating point of the compressor is allowed to move downward and left in terms of a typical compressor map (heat over flow). Since the compressors in Power-to-Ammonia plants are driven by electric machines, this improvement is significant. The compressor power during low availability of renewable energy must be supplied by batteries or fuel cells, which are expensive and can be associated with significant losses.

For reference, when assuming an electrolysis efficiency of 70% [8] (a typical value for low-temperature electrolysis), the HB plant only accounts for approximately 2%–3% of the overall power consumption at full load. However, at times when the HB plant is running near its minimum load, it is likely that the electrolysis is not running at all and hydrogen is supplied from the storage. During these times, the HB plant would be the major power consumer. Moreover, while the power consumption of electrolyzers decreases more than proportional with decreasing load (i.e., electrolysis is more efficient at part load), the opposite is the case for the HB plant. Thus, its relative contribution to the overall plant's power consumption increases at part load. The ASU power consumption at full load is typically lower than that of the HB plant [13].

As the temperature levels of heat rejection and heat supply of the refrigeration cycle are assumed constant, all pressure levels inside the refrigeration cycle are also constant regardless of the loop pressure. This means that the favorable effect described above does not apply to the refrigeration compressors, which can be seen by the almost constant power consumption of the refrigeration compressor in Fig. 8.

For the overall plant scheduling problem, a simple HB plant energy consumption rating must be assumed. Wang et al. [9] assumed that 20% of the compressor power of the HB plant are constant, while 80% scale with the load. Our results show that even with a considerable reduction in loop pressure, we do not get beyond a 50% reduction in compressor power at part load. This is typical of rotating equipment. Other works often assume the power consumption of the HB plant per unit of ammonia produced to be constant in the context of optimal scheduling [5,8,10]. Based on our results, we would argue that for highly flexible plants, the more accurate assumption would be that the total HB power consumption is a linear function of the load that does not reach zero power at 0% load, or even constant. In practice, the

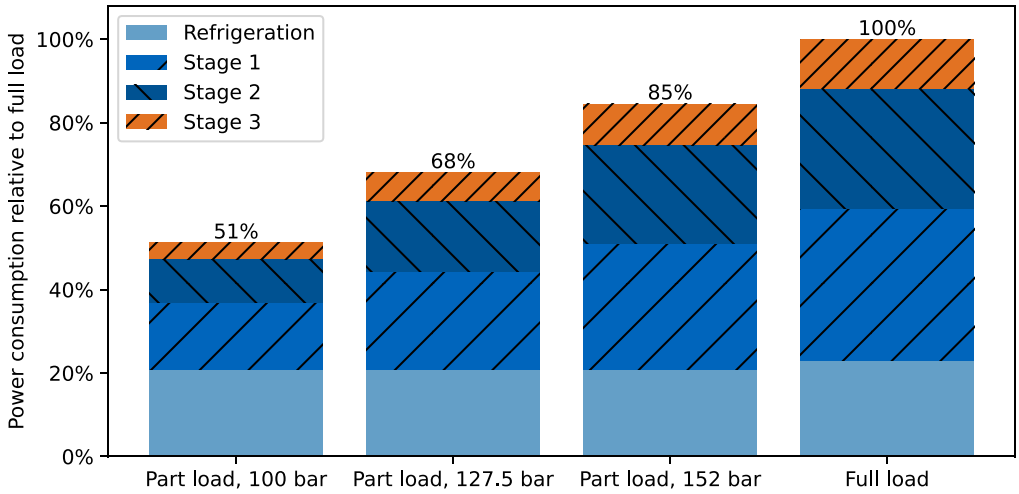

Fig. 8. Power consumption of the HB plant as a function of the part-load pressure compared to full-load power consumption.

power consumption behaves nearly linearly with the load, until the lower ceiling for the operating pressure is met, from where on, it stays approximately constant due to constant pressure ratios and constant volume flows that are maintained by the anti-surge controllers. In a linear program, this HB plant power consumption $P_{\text{HB plant}}$ could be modeled, e.g., by the inequality constraints

$$P_{\text{HB plant}} \geq k_1 * \dot{M}_{\text{H}_2} + k_2 * \dot{M}_{\text{H}_2\,\text{max}} \tag{9}$$

$$P_{\text{HB plant}} \geq P_{\text{HB plant, min}} \tag{10}$$

with the fit parameters k_1, k_2, and $P_{\text{HB plant, min}}$. These parameters depend on the plant design as well as the part-load operating point, particularly the part-load pressure and at which load it is reached. Here, we chose the hydrogen consumption $\dot{M}_{\text{H}_2}$ as the load-determining variable.

4. Summary and outlook

In this work, we demonstrated fast load changes of a HB plant between 10 and 100% load. Load changes were conducted at load change rates of up to ±3%/min. We used some elements of feedforward control based on linear trajectories between two specified operating points. The otherwise largely conventional control structure was able to cope well with the fast load changes and low loads.

Three strategies were investigated. First, keeping all setpoints except for the pressure constant leads to a tenfold reduction in loop mass flow rate, which is challenging for the control structure and instruments. The bed temperatures decrease slightly due to the decreased pressure. Second, operating the reactor without intercooling at part load leads to a higher loop mass flow rate and a moderate increase in reactor bed temperatures. The load change rate is limited by the temperature dynamics of the reactor, but ±3%/min are still possible. Third, additionally increasing the ammonia fraction reduces the bed temperature increase at part load and thereby aids a fast ramp-up. It also leads to significantly higher loop flow, which is favorable for the control system and the gas distribution in the reactor beds.

The pressure was maintained above the specified minimum pressure with all three strategies. We showed that a limited and controlled pressure reduction during part-load operation can significantly reduce the power demand of the HB plant.

The integrated design and scheduling problem, often considered as a linear program, plays an important role for the green ammonia process. As discussed throughout our work, previous works have often made rather conservative assumptions for part load and load change rates of the HB process. These assumptions were based on the operation of conventional plants and adequate in light of the lack of detailed studies on the process level. However, based on the load change rates achieved in our work, the results of recently published scientific articles [19,20] and the claims of major equipment manufacturers and technology firms [37–39], we suggest adjusting the corresponding assumptions in scheduling optimizations in the future. We further proposed modeling equations to describe the load-dependent power demand of the HB plant in a linear program more accurately than the approach used by previous works.

By using advanced control strategies such as MPC or NMPC, even smoother variable trajectories could likely be achieved in the future, lowering the fatigue induced by pressure and temperature changes. Moreover, there is an inherent trade-off between power consumption and equipment fatigue when it comes to the pressure reduction during part-load operation. The intuition here is that the longer a time period of part-load operation, the more worthwhile it is to accept a pressure cycle in exchange for lower power consumption. To our knowledge, this potential optimization problem has not been considered before.

While we have preliminarily validated that our control structure copes well with random load ramps between 10 and 100% load and −3 and +3%/min load change rate, it would be interesting to see the operation of a flexible HB plant following an optimized load trajectory for a given energy system. Such a study could be done in conjunction with a system optimization using assumptions based on our plant design. Similar to Salmon and Bañares-Alcántara [12], a design optimization could be followed by an optimization of the operation with a limited prediction horizon. Finally, the obtained load trajectory could be fed into a fully mechanistic dynamic HB plant simulation.

CRediT authorship contribution statement

Steffen Fahr: Writing – review & editing, Writing – original draft, Visualization, Methodology, Investigation, Conceptualization. **Robert Kender:** Writing – review & editing, Methodology. **Jan-Peter Bohn:** Writing – review & editing, Supervision. **Sebastian Rehfeldt:** Writing – review & editing, Funding acquisition, Conceptualization. **Andreas Peschel:** Writing – review & editing, Supervision, Conceptualization. **Harald Klein:** Writing – review & editing, Supervision, Funding acquisition, Conceptualization.

Declaration of competing interest

The authors declare that they have no known competing financial interests or personal relationships that could have appeared to influence the work reported in this paper.

Acknowledgments

The authors gratefully acknowledge the financial support from the German Federal Ministry of Education and Research (BMBF) through H2Giga SINEWAVE (grant numbers 03HY123A and 03HY123F). We would like to thank Ayan Kumar Bhar for his support with the model development.

Nomenclature

Symbols and corresponding SI units

$\dot{M}$	Mass flow rate	$kg\,s^{-1}$
N	Mole amount	mol
$\dot{N}$	Molar flow rate	$mol\,s^{-1}$
p	Pressure	Pa
P	Power	$J\,s^{-1}$
$\bar{R}$	Universal gas constant	$J\,mol^{-1}\,s^{-1}$
t	Time	s
T	Temperature	K
V	Volume	m^3
w_i	Mass fraction of component i	-
X_{diss}	Molar loading of dissolved gases	-
λ	Plant load	-
ν	Stoichiometric coefficient	-
ξ	Reaction extent	mol
$\dot{\xi}$	Reaction rate	$mol\,s^{-1}$

Abbreviations

ASU	Air separation unit
eFEHE	External feed-effluent heat exchanger
HB	Haber–Bosch
HP	High-pressure
iFEHE	Internal feed-effluent heat exchanger
LAC^{TM}	Linde Ammonia Concept
LCOA	Levelized cost of ammonia
LP	Low-pressure
MP	Medium-pressure
MPC	Model-predictive control
NMPC	Nonlinear model-predictive control
OP	Controller output
PFD	Process flow diagram
PFR	Plug flow reactor
PV	Controller process variable
SP	Controller setpoint

References

[1] Egerer J, Grimm V, Niazmand K, Runge P. The economics of global green ammonia trade — "Shipping Australian wind and sunshine to Germany". Appl Energy 2023;334:120662. http://dx.doi.org/10.1016/j.apenergy.2023.120662.

[2] Weikl M, Peschel A. Industrial view on hydrogen carriers for intercontinental transport. Curr Opin Green Sustain Chem 2023;100843. http://dx.doi.org/10.1016/j.cogsc.2023.100843.

[3] Brown T. MAN energy solutions: An ammonia engine for the maritime sector. 2019, URL: https://ammoniaenergy.org/articles/man-energy-solutions-an-ammonia-engine-for-the-maritime-sector/. [Accessed 13 June 2024].

[4] Hignett TP. Transportation and storage of ammonia. In: Fertilizer manual. Springer; 1985, p. 73–82.

[5] Salmon N, Bañares-Alcántara R. Impact of grid connectivity on cost and location of green ammonia production: Australia as a case study. Energy Environ Sci 2021;14(12):6655–71. http://dx.doi.org/10.1039/D1EE02582A.

[6] Kender R, Rößler F, Wunderlich B, Pottmann M, Thomas I, Ecker A-M, et al. Improving the load flexibility of industrial air separation units using a pressure–driven digital twin. AIChE J 2022;68(7). http://dx.doi.org/10.1002/aic.17692.

[7] Mucci S, Mitsos A, Bongartz D. Power-to-X processes based on PEM water electrolyzers: A review of process integration and flexible operation. Comput Chem Eng 2023;175:108260. http://dx.doi.org/10.1016/j.compchemeng.2023.108260.

[8] Armijo J, Philibert C. Flexible production of green hydrogen and ammonia from variable solar and wind energy: Case study of Chile and Argentina. Int J Hydrog Energy 2020;45(3):1541–58. http://dx.doi.org/10.1016/j.ijhydene.2019.11.028.

[9] Wang C, Walsh SDC, Longden T, Palmer G, Lutalo I, Dargaville R. Optimising renewable generation configurations of off-grid green ammonia production systems considering Haber–Bosch flexibility. Energy Convers Manage 2023;280:116790. http://dx.doi.org/10.1016/j.enconman.2023.116790.

[10] Campion N, Nami H, Swisher PR, Vang Hendriksen P, Münster M. Techno-economic assessment of green ammonia production with different wind and solar potentials. Renew Sustain Energy Rev 2023;173:113057. http://dx.doi.org/10.1016/j.rser.2022.113057.

[11] Smith C, Torrente-Murciano L. The importance of dynamic operation and renewable energy source on the economic feasibility of green ammonia. Joule 2024;8(1):157–74. http://dx.doi.org/10.1016/j.joule.2023.12.002.

[12] Salmon N, Bañares-Alcántara R. Impact of process flexibility and imperfect forecasting on the operation and design of Haber–Bosch green ammonia. RSC Sustain 2023;1(4):923–37. http://dx.doi.org/10.1039/D3SU00067B.

[13] Florez J, AlAbbad M, Vazquez-Sanchez H, Morales MG, Sarathy SM. Optimizing islanded green ammonia and hydrogen production and export from Saudi Arabia. Int J Hydrog Energy 2024;56:959–72. http://dx.doi.org/10.1016/j.ijhydene.2023.12.075.

[14] Fahr S, Schiedeck M, Schwarzhuber J, Rehfeldt S, Peschel A, Klein H. Design and thermodynamic analysis of a large-scale ammonia reactor for increased load flexibility. Chem Eng J 2023;471:144612. http://dx.doi.org/10.1016/j.cej.2023.144612.

[15] Fahr S, Schiedeck M, Reinke M, Bohn J-P, Rehfeldt S, Peschel A, et al. Simultaneous design and part-load optimization of an industrial ammonia synthesis reactor. Chem Eng J 2024;480:148302. http://dx.doi.org/10.1016/j.cej.2023.148302.

[16] Cheema II, Krewer U. Optimisation of the autothermal NH3 production process for power-to-ammonia. Processes 2020;8(1):38. http://dx.doi.org/10.3390/pr8010038.

[17] Khademi MH, Sabbaghi RS. Comparison between three types of ammonia synthesis reactor configurations in terms of cooling methods. Chem Eng Res Des 2017;128:306–17. http://dx.doi.org/10.1016/j.cherd.2017.10.021.

[18] Wang G, Mitsos A, Marquardt W. Conceptual design of ammonia-based energy storage system: System design and time-invariant performance. AIChE J 2017;63(5):1620–37. http://dx.doi.org/10.1002/aic.15660.

[19] Rosbo JW, Ritschel TKS, Hørsholt S, Huusom JK, Jørgensen JB. Flexible operation, optimisation and stabilising control of a quench cooled ammonia reactor for power-to-ammonia. Comput Chem Eng 2023;176:108316. http://dx.doi.org/10.1016/j.compchemeng.2023.108316.

[20] Rosbo JW, Jensen AD, Jørgensen JB, Huusom JK. Comparison, operation and cooling design of three general reactor types for power-to-ammonia processes. Chem Eng J 2024;496:153660. http://dx.doi.org/10.1016/j.cej.2024.153660.

[21] Kelley MT, Do TT, Baldea M. Evaluating the demand response potential of ammonia plants. AIChE J 2022;68(3). http://dx.doi.org/10.1002/aic.17552.

[22] Araújo A, Skogestad S. Control structure design for the ammonia synthesis process. Comput Chem Eng 2008;32(12):2920–32. http://dx.doi.org/10.1016/j.compchemeng.2008.03.001.

[23] Luyben WL. Design and control of a cooled ammonia reactor. In: Rangaiah GP, Kariwala V, editors. Plantwide control: Recent developments and applications, vol. Recent Developments and Applications. John Wiley & Sons; 2012, http://dx.doi.org/10.1002/9781119968962.ch13.

[24] Kong B, Zhang Q, Daoutidis P. Nonlinear model predictive control of flexible ammonia production. Control Eng Pract 2024;148:105946. http://dx.doi.org/10.1016/j.conengprac.2024.105946.

[25] Ostuni R, Zardi F. Method for load regulation of an ammonia plant. 2015, EP2589574B1.

[26] Linde Engineering. Linde to build large ammonia plant in Russia. 2013, URL: https://www.linde-engineering.com/en/news_and_media/press_releases/news_20130528.html. [Accessed 12 June 2024].

[27] Fischer KL, Freund H. On the optimal design of load flexible fixed bed reactors: Integration of dynamics into the design problem. Chem Eng J 2020;393:124722. http://dx.doi.org/10.1016/j.cej.2020.124722.

[28] Bruns B, Herrmann F, Grünewald M, Riese J. Dynamic design optimization for flexible process equipment. Ind Eng Chem Res 2021;60(20):7678–88. http://dx.doi.org/10.1021/acs.iecr.1c00306.

[29] Honeywell. UniSim design operations guide: R491 release. 2022.

[30] Flórez-Orrego D, de Oliveira Junior S. Modeling and optimization of an industrial ammonia synthesis unit: An exergy approach. Energy 2017;137:234–50. http://dx.doi.org/10.1016/j.energy.2017.06.157.

[31] Knudsen LB. Dynamic ammonia synthesis. In: Nitrogen + syngas conference. 2024, Munich, Germany, 2024/03/05.

[32] Speth CH, Hulqvist M, Han PA. Method for the control of pressure in a loop for the preparation of ammonia or methanol. 2021, WO2021233780A1.

[33] Liu L, Tian S, Xue D, Zhang T, Chen Y. Industrial feedforward control technology: A review. J Intell Manuf 2019;30(8):2819–33. http://dx.doi.org/10.1007/s10845-018-1399-6.

[34] Cheema II, Krewer U. Operating envelope of Haber–Bosch process design for power-to-ammonia. RSC Adv 2018;8(61):34926–36. http://dx.doi.org/10.1039/C8RA06821F.

[35] Allman A, Palys MJ, Daoutidis P. Scheduling–informed optimal design of systems with time–varying operation: A wind–powered ammonia case study. AIChE J 2019;65(7). http://dx.doi.org/10.1002/aic.16434.

[36] Verleysen K, Parente A, Contino F. How sensitive is a dynamic ammonia synthesis process? Global sensitivity analysis of a dynamic Haber–Bosch process (for flexible seasonal energy storage). Energy 2021;232:121016. http://dx.doi.org/10.1016/j.energy.2021.121016.

[37] Ostuni R, Bialkowki M, Corbetta M. Dynamic analysis of casale Green ammonia. 2021, URL: https://www.ammoniaenergy.org/wp-content/uploads/2021/11/Casale-slides-AEA-21-published.pdf.

[38] Green ammonia solutions: Made to withstand feedstock fluctuations. 2024, URL: https://www.topsoe.com/processes/green-ammonia.

[39] Beach J, Kintner J, Welch A. Rapid ramp NH3 reactor update. 2018, URL: https://nh3fuelassociation.org/wp-content/uploads/2018/12/1600-Starfire-Energy_NH3FA-technical_Joe-Beach_2018-10-31_v08.pdf. [Accessed 12 June 2024].